Formation of polymer brushes inside cylindrical pores: A computer simulation study

Alexandros G. Koutsioubas,[a] Nikolaos Spiliopoulos, Dimitris L. Anastassopoulos, Alexandros A. Vradis,[b] and Chris Toprakcioglu
Department of Physics, University of Patras, Patras 26500, Greece

(Received 2 April 2009; accepted 24 June 2009; published online 22 July 2009)

The formation process of polymer brushes, formed by the adsorption of flexible end-functionalized chains from dilute solutions on the inner surface of cylindrical pores is studied by bond fluctuation Monte Carlo simulations. Various properties as the grafting density, monomer, and free-end distribution are monitored as a function of pore diameter D and chain length N. Two different modes of end-segment attachment on the inner pore surface are considered: (a) pure-irreversible "hard" grafting and (b) irreversible "soft" grafting where grafted-ends can move freely on the pore surface but cannot detach from it. Different regimes of pore coating are indentified, depending on the mode of end-segment attachment and on the ratio of D to the radius of gyration of the free polymer chains in solution R_g. These initial findings can be used as a guide for the preparation of actual polymer brushes inside ordered porous membranes by the "grafting to" approach. © *2009 American Institute of Physics*. [DOI: 10.1063/1.3179686]

I. INTRODUCTION

Flexible polymer chains end-tethered to a surface at sufficiently high grafting densities tend to extend away from the surface due to excluded volume interactions. This extension, which is counterbalanced by an elastic restoring force of entropic origin, leads to the formation of a layer of stretched chains referred to as a "polymer brush." These systems have been the subject of extensive theoretical and experimental investigations[1–5] due to their widespread use in colloidal stabilization, adhesion, wetting, lubrication, and in general the modification of surface properties.

Although the vast majority of published works concern polymer brushes on flat substrates,[6–8] the properties of polymer brushes grown on convex or concave interfaces have also been investigated[9–14] together with the behavior of chains confined inside narrow tubes and slits.[15–21] Polymer brushes on curved surfaces represent a system of both theoretical and practical interests. Notable examples include brush formation on rough surfaces,[22] polymer coated colloidal particles,[23] polymer decorated nanotubes,[24] modulation of electro-osmotic flow by end-grafted polymer chains,[25] and brush-based pressure-sensitive microvalves.[26]

While polymer brushes on flat substrates can be treated to a first approximation as a linear string of blobs of equal size,[27,28] in the case of nonplanar surfaces, changes in the space available for each grafted chain due to curvature complicate the theoretical treatment. Following the classic analysis of Daoud and Cotton[29] for star polymers, brushes on curved surfaces can be envisioned as an array of concentric shells of blobs that have variable sizes, depending on their distance from the grafting surface. In this framework, when the radius of curvature of the grafting surface is much larger than the characteristic lengths (height L_0, interanchor distance s) of the polymer brush, the overall properties are expected to approximate those of a brush on a flat substrate. On the other hand for large curvatures (i.e., small radii of curvature), deviations from the flat brush behavior become more pronounced.

The convex or concave nature of the grafting surface produces different effects on the brush structure. In the case of positive curvatures (convex geometry) the deformation energy is lowered with respect to the flat brush case. On the contrary negative curvatures (concave geometry) lead to increased chain confinement. For brushes grafted inside spheres or cylinders, different regimes of confinement have been predicted[9] depending on grafting density σ, chain length N, and sphere/cylinder diameter D.

In 2006 Dimitrov *et al.*[13] presented molecular dynamics simulations of polymer brushes inside cylindrical pores for a broad range of σ, N, and D parameters and compared their results with scaling theoretical arguments. They have identified different regimes inside the pore such as mushrooms, cigars, compressed cigars, overlapping cigars, compressed brushes, and "normal" brushes that are characterized by distinct power laws. These power laws provide a connection between the linear dimensions of the chains and brush height in terms of the parameters σ, N, and D and may serve as a general guide for this rather complex behavior.

The preparation of poly(methyl methacrylate) polymer brushes inside porous membranes, such as porous anodic alumina and porous silicon, by "grafting from" methods has been studied recently.[30] It was found that due to confinement effects imposed by the pores, the resulting brushes are characterized by a large polydispersity while large chain molecular weight cannot be achieved. So the "grafting to" or "brush self-assembly from solution" method may be more appropri-

[a]Present address: Laboratoire Léon Brillouin, CEA SACLAY, 91191 Gif-sur-Yvette Cedex, France.
[b]Electronic mail: vradis@physics.upatras.gr.

ate for brush formation inside cylindrical pores, despite the fact that high grafting densities are difficult to achieve.

Motivated by the potential practical interest in the preparation of self-assembled brushes inside porous membranes and other relevant applications,[31] we have carried out bond fluctuation Monte Carlo (BFMC) simulations of end-functionalized chain adsorption on the inner surface of cylindrical pores from bulk solutions. For a range of systems with different chain lengths N and pore diameters D, we have monitored the evolution of the grafting density σ inside the pore and the structural properties (monomer density profile, free end distribution) of the resulting confined brushes. Furthermore, two different modes of end-segment attachment on the inner pore surface are considered: (a) "hard" irreversible grafting and (b) "soft" irreversible grafting with grafted-end movement on the pore walls. Our simulations show that these two different modes produce two distinct behaviors, a fact that should be relevant to experimental realizations of polymer brushes inside ordered porous membranes.

II. MODEL AND SIMULATION METHODOLOGY

We have adopted a lattice BFMC technique that has been originally proposed by Carmesin and Kremer[32] and has been used for the study of end-grafted brushes.[33–36] This model has also been implemented for the study of adsorption kinetics from bulk solutions of homopolymer[37] and end-functionalized chains on flat surfaces.[38–40] The BFMC technique possesses the typical computational advantages of lattice MC methods; the asymptotic limit of power laws related to chain behavior is reached for relatively small chain contour lengths while Rouse chain dynamics are adequately reproduced[41] in the dilute regime and under good solvent conditions.

Briefly, in the BFMC model for polymer chains in good solvent conditions, each monomer occupies a cube of eight lattice sites on a cubic lattice. Each MC step involves a random local displacement in one randomly selected direction of a random monomer and the implementation of the excluded volume and bond length criterion. The allowed bond vectors connecting two neighboring monomers may only have a length equal to 2, $\sqrt{5}$, $\sqrt{6}$, 3, or $\sqrt{10}$.[42] The choice of this set of bond vectors ensures that two bonds cannot cross each other.

In our model N_p monodisperse chains, each consisting of $N+1$ monomers are randomly placed inside two cubic solution reservoirs of $L_x \times L_y \times L_z$ volume each where $L_x=L_y=L_z=200$. These two reservoirs are connected by a cylindrical pore of diameter D and length L (Fig. 1). The main body of our simulations was performed for $L=100$ while some additional simulations were performed for $L=50$ and $L=200$. The concentration c inside each reservoir is set equal to 0.025 that corresponds to a dilute solution. Thus the total number of chains inside each reservoir is given by $N_p/2=(L_x \cdot L_y \cdot L_z \cdot c)/8(N+1)$ while the total number of monomers in our simulations is 5×10^4. Due to the large volume of the solution reservoirs as compared to the pore dimensions, adsorption of chains inside the pore does not appreciably change the reservoir solution concentration in all our simulations.

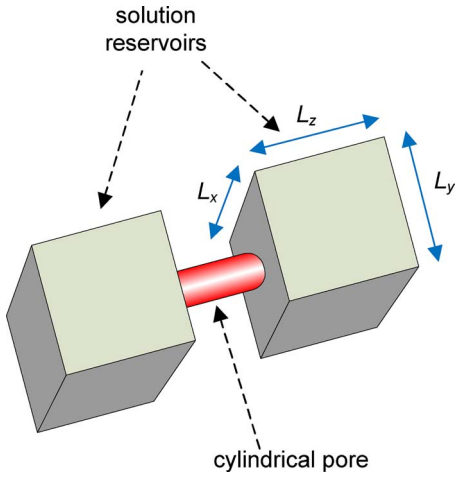

FIG. 1. Schematic illustration of the system under study.

Initially the polymer chains inside the reservoirs are equilibrated by performing 4×10^7 MC steps per monomer (MC cycles). During equilibration, chains are not allowed to enter inside the cylindrical pore and their radius of gyration R_g and end-to-end distance R_e is measured (Table I). After equilibration, chains are left free to enter the pore while one of their two terminal monomers may adsorb irreversibly on the pore walls. To model the adsorption of the end-functionalized chains onto the pore walls two different grafting-modes are investigated: (a) hard irreversible grafting where a functionalized end-monomer lying on the pore wall cannot move and (b) soft irreversible grafting where a functionalized end-monomer lying on the pore wall can move on the wall surface but cannot depart from the pore wall. The lattice sites that compose the pore walls are those having a radial distance d from the cylinder axis that fulfills the inequality $D/2 \leq d < (D/2)+1$.

For each system $10^8 - 2 \times 10^8$ MC cycles are performed, in order to monitor chain adsorption. Note that for every chain length, the total simulation time is 4–5 orders of magnitude higher than the chain relaxation time[35] while the rms displacement of the chain center of mass is at least ten times larger than the pore length. Several quantities of interest are calculated during chain adsorption such as the grafting density σ, the monomer $\phi(r)$, and free-end $\rho(r)$ distribution of the grafted chains as a function of the distance from the cylinder axis r and the monomer concentration along the cylinder axis. All these quantities are also monitored for the inner half of the pore surface.

TABLE I. Radius of gyration R_g and end-to-end distance R_e of the chains after system equilibration for a monomer concentration inside the solution reservoirs equal to 0.025.

	$N=5$	$N=10$	$N=20$	$N=40$
R_g	2.4	3.8	5.7	8.7
R_e	6.2	9.6	14.6	21.8

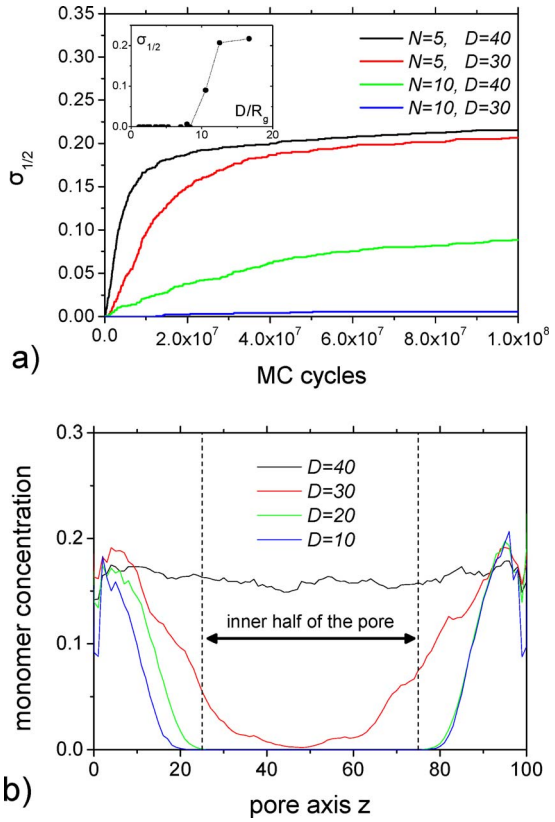

FIG. 2. Hard grafting adsorption case for pore length $L=100$. (a) Adsorption kinetics in the inner half of the pore for the four pairs of simulation parameters ($D=40$, $N=10$), ($D=40$, $N=5$), ($D=30$, $N=5$), and ($D=30$, $N=10$). Note that for any other pair(D, N), grafting density on the inner half of the pore, $\sigma_{1/2}$, is zero. In the inset, the grafting density after 10^8 MC cycles on the inner half of the pore $\sigma_{1/2}$ is plotted as a function of the ratio D/R_g. (b) Monomer concentration along pore axis for $N=10$ after 10^8 MC cycles. Note that only for $D=40$ a uniform concentration is achieved along the pore. For lower pore diameters chains adsorb only near the pore openings creating a barrier for incoming chains.

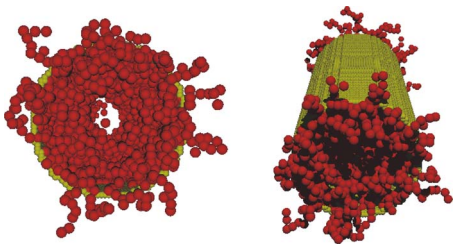

FIG. 3. Simulation snapsot for system parameters $D=40$, $N=10$ in the case of hard grafting. Note that near the cylinder axis an empty narrow aperture for incoming chains is available. Monomer concentration is also high outside the pore space due to grafted chains that are repelled outside the pore.

III. RESULTS AND DISCUSSION

Intuitively we expect that chain diffusion and adsorption on the inner part of the pore depend on the relative size of the pore diameter and the chain length. For large values of N where chain dimensions are comparable or slightly larger than the pore diameter, entropic restrictions should prevent their approach inside the pore. Furthermore, adsorption of chains on the pore openings adds another obstacle that prohibits chain diffusion inside the pore. This latter effect is expected to be more pronounced in the case of hard grafting where functionalized end-monomers cannot move along the pore walls.

In Fig. 2(a), we present the kinetics of chain adsorption on the inner half of the pore (grafting density $\sigma_{1/2}$ versus time MC cycles) in the case of hard grafting with $L=100$ for various combinations of D and N. We observe that the grafting density $\sigma_{1/2}$ gets lower as the number of monomers per chain increase, an effect that is also observed in the case of brush formation on flat surfaces.[39] This happens because longer chains are characterized by a large unperturbed size that allows only for low crowding of the brush layer.

The most pronounced effect that is reflected on the kinetics of hard grafting is that grafting density $\sigma_{1/2}$ falls almost to zero for every combination of D and N, except for the three pairs ($D=40$, $N=10$), ($D=40$, $N=5$), and ($D=30$, $N=5$). Note that even for chains with $N=10$ that have a radius of gyration $R_g=3.8$, grafting inside a relatively wide pore with $D/2=15$ cannot take place. Obviously, on size considerations alone, individual chains are able to enter the pore since their size in solution is much smaller than the pore size. Their inability to form a brush on the inner pore surface, however, can only be attributed to the formation of a densely populated barrier on the pore openings that repels incoming chains—an effect that might be described as "pore-plugging."

A plot of the mean monomer density along the pore axis [Fig. 2(b)] reveals that there is always a large monomer density near the pore openings [both inside and outside the pore space (see Fig. 3)]. This "barrier layer" is formed very quickly since the first chains that enter the pore, most likely graft near the pore openings. Uniform grafting along the pore axis can only take place when the ratio D/N is large enough so that near the pore axis the barrier layer has a low monomer concentration and an aperture for incoming chains is available (Fig. 3).

A simple examination of the results in Fig. 2(a) reveals that when the ratio D/R_g is less than about nine, chain adsorption on the inner part of the pore is almost totally blocked within the accessible simulation time. On the other hand for $D/R_g>9$ uniform pore grafting can take place but the time needed for brush formation still depends on the size of the pore. For example, note in Fig. 2(a) that for $N=5$ and $D=30$ or $D=40$, $\sigma_{1/2}$ is approaching almost the same value but at a clearly different rate, which is an ascending function of D.

Simulations for even longer pores with $L=200$ show again that chains are able to diffuse and graft on the inner pore surface only when $D/R_g>9$ [Figs. 4(a) and 4(b)]. The only effect that is produced by the larger pore length is the obvious slowing down of adsorption kinetics. Note that even in simulations of short pores ($L=50$), results not shown here, where pore length and diameter is comparable, strict uniform pore grafting cannot take place for $D/R_g<9$ after 2×10^8 MC cycles.

For the three pairs of system parameters for which uniform chain grafting along the pore is achieved, we plot the xy projection of the monomer density inside the pore (Fig. 5). Apart from a model inherent small depletion layer[33] near the pore surface, monomer density falls smoothly as we ap-

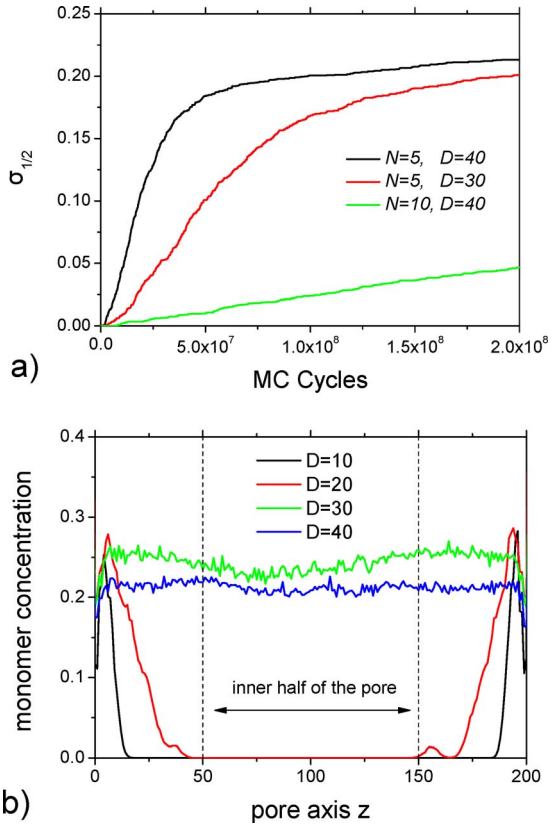

FIG. 4. Hard grafting adsorption case for a pore length $L=200$. (a) Adsorption kinetics in the inner half of the pore for the three pairs of simulation parameters ($D=40$, $N=10$), ($D=40$, $N=5$), and ($D=30$, $N=5$). Note that for any other pair (D, N), grafting density on the inner half of the pore $\sigma_{1/2}$ is zero. (b) Monomer concentration along pore axis for $N=5$ and various pore diameters after 2×10^8 MC cycles.

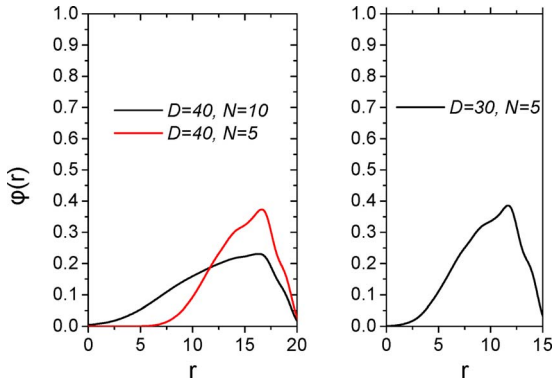

FIG. 6. Radial monomer distribution profiles inside the inner half of the pore in the case of hard grafting.

proach the pore axis, while maximum density is observed at about 3 to 4 lattice spacings from the pore surface. Near the pore axis, an almost monomer-free cylindrical cavity is present whose diameter depends on the ratio D/N. As we have commented above this monomer-free space acts as a "passage" for incoming chains.

The observed plateaus of the grafting density $\sigma_{1/2}$ in Figs. 2(a) and 4(a) suggest that the grafted layers are in the semidilute brush regime, since the calculated mean interanchor distances s of the grafting points are smaller than the critical value $1.4R_g$.[35] Valuable information is also included in plots of the radial monomer density $\phi(r)$ and free-end density $\rho(r)$ (Figs. 6 and 7). The radial monomer density profiles are typical of polymer brush behavior and can be compared with molecular dynamics results of Dimitrov *et al.*[12–14] The distribution has a parabolic shape and a characteristic decaying tail is present. Also we observe that the free-ends of the chains populate the whole grafted layer while the maximum of their distribution is located near the decaying tail of the monomer density profile. We emphasize that in the limiting case where $D=40$, $N=10$ with $D/R_g=10$ the free-end distribution has a nonvanishing value at $r=0$. This means that near the critical value $D/R_g=9$ a small fraction of the grafted chains are so stretched that their free-ends have a distance more than $D/2$ from the grafting surface.

Now we turn to the case of soft grafting inside the pore. In Fig. 8, we present the kinetics of chain adsorption (grafting density $\sigma_{1/2}$ vesus time MC cycles) on the inner half of the pore with $L=100$ in the case of soft grafting for representative combinations of D and N. By making a comparison with the kinetics of hard grafting [Fig. 2(a)], two major differences are easily identified: (a) adsorption rates are much higher for soft grafting and (b) even large chains are able to uniformly graft along relatively narrow pores despite the fact that final grafting densities are quite low.

These differences are a direct result of the different mechanisms of chain adsorption under the soft grafting model. The ability of grafted-ends to diffuse along the cylindrical pore surface leads to uniform pore filling (Fig. 9). As in the case of hard grafting, the first incoming chains are

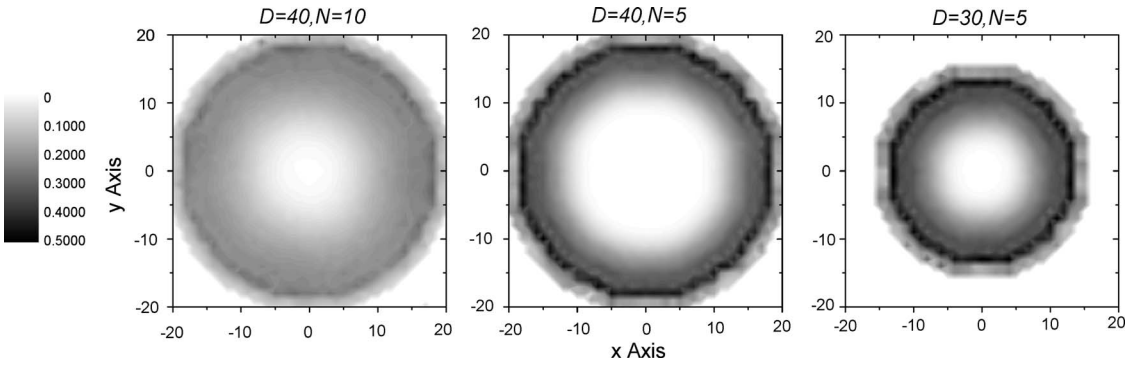

FIG. 5. Contour plots of the xy projection of the monomer density (averaged over the z-direction) inside the inner half of the pore for the hard grafting case ($L=100$).

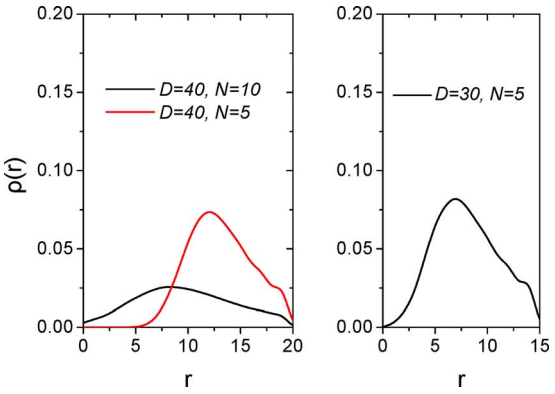

FIG. 7. Radial free-end distribution profiles inside the inner half of the pore in the case of hard grafting.

grafted near the pore openings forming a monomer-rich area. Due to excluded volume interactions and since these grafted chains cannot desorb, they move toward the inner monomer-free pore space making room for other incoming chains. As MC cycles advance, monomer density inside the pore gets higher making it difficult for other chains to adsorb. It is interesting to note that when $D/R_g > 9$, the final values of $\sigma_{1/2}$ are approximately the same for both hard and soft grafting.

In Fig. 10, representative contour plots of the xy projection of the monomer density inside the inner half of a pore for $N=10$ are presented. We observe that as the pore diameter decreases, pore space gets evenly filled by monomers and the area near the pore axis gets crowded in contrast to the picture of hard grafting. Radial plots of the monomer $\phi(r)$ and free-end $\rho(r)$ density profiles (Figs. 11 and 12) also reflect this trend. We see that as D/R_g gets much lower than the value 9, both $\phi(r)$ and $\rho(r)$ at $r=0$ are nonzero. This enhanced monomer and free-end concentration on the pore axis indicates that chains are not confined only inside the semicylinder where one of their ends is grafted but they interact with other chains that are grafted on the opposite semicylinder (brush interdigitation). In this regime, especially the shape of the free-end distribution is largely affected having a distribution maximum at $r=0$ (Fig. 13) and being a descending function of r. The values $\phi(0)$ and $\rho(0)$ may serve as an indirect measure of the overall brush interdigitation inside the pore. Again for $D/R_g > 9$, the shape of $\phi(r)$ and $\rho(r)$ is identical for both grafting models.

In Figs. 2(a), 4(a), and 8 we see that both hard and soft grafting adsorption kinetics, include a wide spectrum of time scales. In the case of the soft grafting model, the log-log

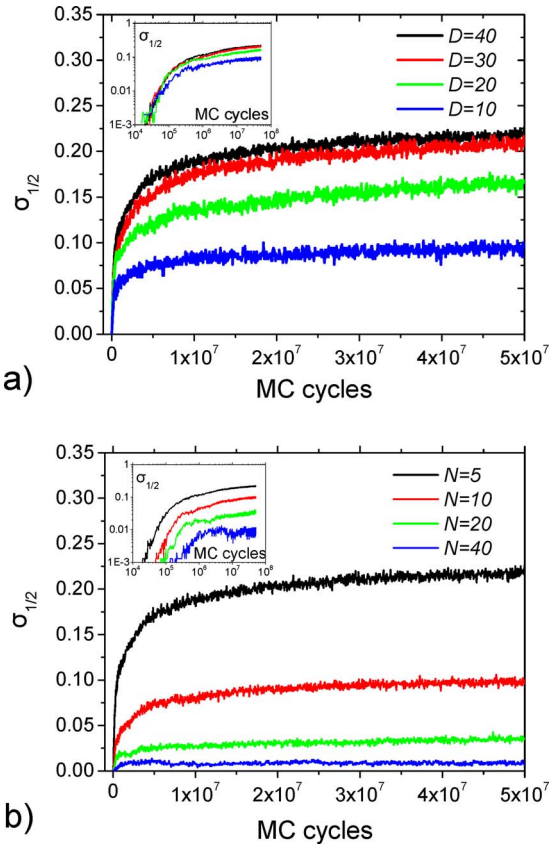

FIG. 8. Representative self-assembly kinetics in the case of soft grafting inside the inner half of the pore ($L=100$) for (a) $N=5$ and $D=10$, 20, 30, 40 and (b) $D=40$ and $N=5$, 10, 20, 40. In each inset, the log-log plot of adsorption kinetics is presented.

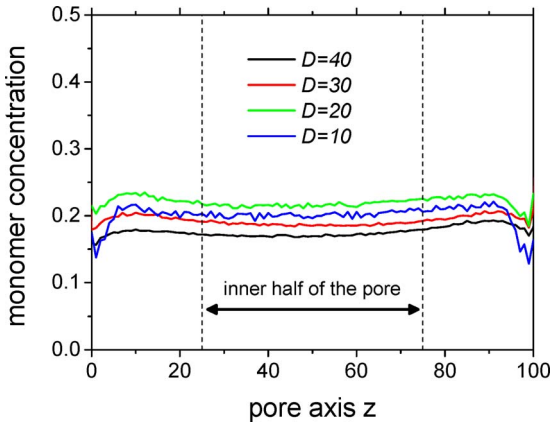

FIG. 9. Monomer concentration along pore axis ($L=100$) for $N=10$ in the case of soft grafting after 10^8 MC cycles. Contrary to hard grafting [Fig. 2(b)], for every pore diameter an almost uniform concentration of the same order is achieved across the pore.

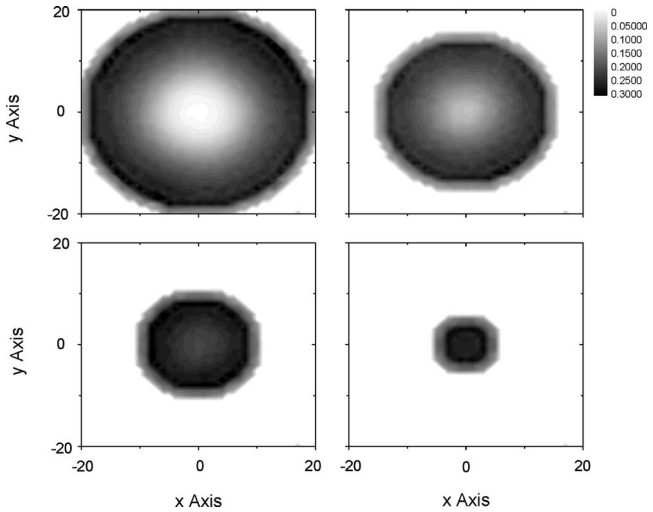

FIG. 10. Contour plots of the xy projection of the monomer density (averaged over the z-direction) inside the inner half of a pore with $D=40$, 30, 20, 10 and $N=10$ in the soft grafting case.

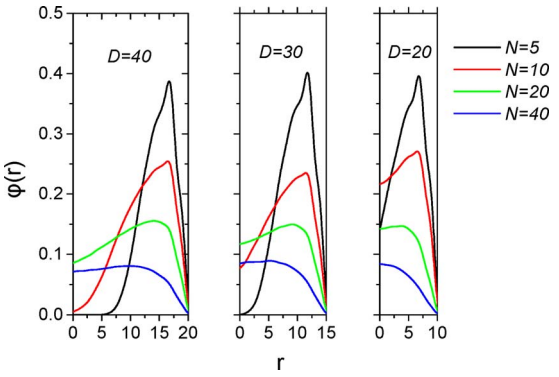

FIG. 11. Radial monomer distribution profiles inside the inner half of the pore in the case of soft grafting.

plots of the kinetics curves (Fig. 8) reveal that there are two clearly separate stages during brush formation inside the pore. These two stages can be attributed to the existence of different adsorption mechanisms during early and late times of adsorption. It is interesting to note, that the transition time between early (fast) and late (slow) kinetics is primarily dependent on the number or monomers per chain N.

Even after $10^8-2\times10^8$ MC cycles, equilibrium has not yet been fully reached and a very slow population of the adsorbed layer still takes place. The characteristic times of chain adsorption and diffusion toward a flat surface have been studied previously by the BFMC method.[38,39] Here due to the special geometry of the system, the limiting factor that dominates the kinetics of the hard grafting case is the characteristic time of chain diffusion through the concentration barrier near the pore openings. Clearly the time needed for the penetration of this concentration barrier for $D/R_g<9$ is much higher than that of chain diffusion along the pore and chain adsorption on the pore walls. Quantitatively we may estimate the characteristic adsorption time τ on the inner half of the pore by fitting the $\sigma_{1/2}(t)$ kinetic curves with a generalized stretched exponential form as described by Jia and Lai.[37] For $D/R_g>9$ (both for the hard and soft models) we find a systematic decrease in τ with increasing D/R_g.

For longer pores ($L=200$) under the hard grafting model, the characteristic adsorption time τ increases since incoming chains have to diffuse along the longer pore and also penetrate the preformed brush layer in order to adsorb. Of course, the pore-plugging effect for $D/R_g<9$ is not an equilibrium state of the system. However chain diffusion through the high concentration barrier is so slow that for the accessible simulation time no adsorption takes place on the inner pore surface. We expect that in real experiments, pore-plugging may manifest itself either as the absence of appreciable measured adsorption after long adsorption times, or in situations where the spatial variation of concentration inside pores can be probed, as extremely slow population of the inner surface of the pore.

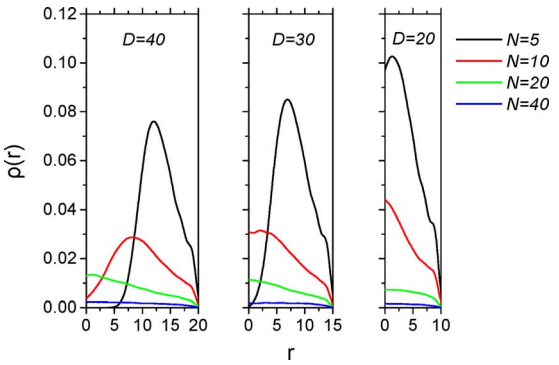

FIG. 12. Radial free-end distribution profiles inside the inner half of the pore in the case of soft grafting.

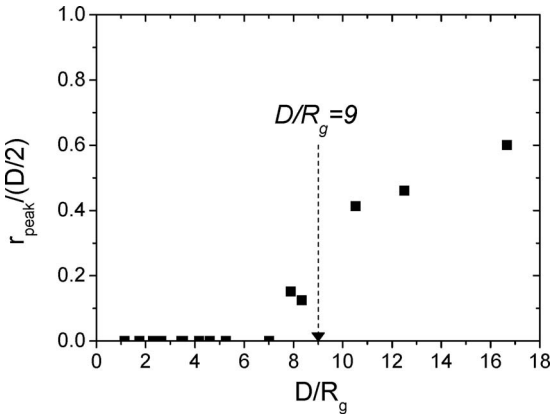

FIG. 13. Radial position of the free-end distribution maximum r_{peak} as a function of D/R_g (soft grafting case). Note that as D/R_g becomes lower than ca. 9, the free-end distribution peak is positioned very close to or on the pore axis ($r=0$).

In this work we have examined chain adsorption inside cylindrical pores for a range of D/R_g from about 1 to 17. The behavior of longer chains in very narrow tubes ($D/R_g\ll1$) is also a very interesting subject, not entirely in the context of adsorption but rather in the context of single chain dynamics and translocation through nanochannels.[43–46] We note that in this regime of strong chain confinement, pore filling is largely unfavored due to the large free energy increase, which gives rise to a constant extrusion force acting on the chain.[43] Simulations of systems in the limit $D/R_g>15$ can give further information and a connection with theoretical scaling arguments concerning brush formation may be established. However the simulation time needed in order to sample the (D, N) parameter space would be much increased.

Further generalizations of the present study may include simulation of much larger systems, which better reflect the properties of real polymer chains, simulation of brush adsorption via a finite energy attraction of end-functionalized monomers on the pore wall,[39] and the inclusion of chain adsorption on the flat surface surrounding the pore openings. Such updates of the model should offer a more realistic description of polymer brush self-assembly in ordered porous membranes. Also the effect of poorer solvent on the adsorption process may be investigated using the BFMC model by the inclusion of attractive interactions between nonbonded neighboring monomers.[34] Since chain size in poorer solvents is smaller as compared to the good solvent case, it is a possibility that brush formation inside the pore for $D/R_g<9$ may take place.

The simulation results for $L=200$ suggest that our conclusions concerning "pore plugging" for $D/R_g<9$ also apply when adsorption inside much longer pores ($L\gg D$) is consid-

ered, which is a case of practical interest. The effect of pore plugging primarily depended on the behavior of the early adsorbed chains near the pore entrance that is taken into account explicitly in our simulations. It is worth pointing out that the observed plugging effect bears some resemblance to the jamming phenomenon that has been reported[47,48] in granular flow systems, where the jamming probability presents an abrupt increase as the tube diameter reaches a critical value.

Our observations on the differences between hard and soft grafting modes are related to the nature of the functional end-groups that are usually used in experimental studies of self-assembled brushes.[6] Obviously the mobility of the end-group on the pore surface would play a crucial role on the overall pore filling. Since brush coated cylindrical pores are promising candidates for some intriguing applications[23–26] and are also related to interesting biosystems (e.g., adsorbed proteins inside biomembranes), this preliminary study may offer some insights toward the experimental realization of such systems.

IV. CONCLUSIONS

The adsorption process of flexible polymers end-grafted on the inner walls of cylindrical pores from dilute solutions was studied by BFMC simulations. Two different modes of irreversible grafting are considered, namely, soft and hard grafting. For the case of hard grafting two different regimes are identified: (a) a slowly evolving uniform grafting along the pore axis for $D/R_g > 9$ and (b) an absence of grafted chains on the inner pore surface for $D/R_g < 9$ caused by the formation of a barrier layer on the pore openings. On the contrary when soft grafting is considered, a small number of large chains are able to end-graft on the inner pore surface at relatively short times. This is due to the different mechanisms of adsorption that includes chain grafting near the pore openings and subsequent diffusion of grafted-ends toward the inner pore surface.

When a uniform grafting is achieved, our simulations yield the monomer and free-end radial density profiles for the inner pore space. The obtained profiles are typical of polymer brush behavior while they provide information for the average chain extension from the grafting wall and the overall chain confinement. Although the simulation model we have used is simple and only relatively small chains are considered, we argue that the present results capture the essentials of chain adsorption inside cylindrical tubes and may offer a general guide for the experimental study of polymer brush formation inside ordered porous membranes such as nanoporous alumina and porous silicon.

[1] *In Polymers at Interfaces*, edited by G. J. Fleer, M. A. Cohen Stuart, J. M. H. M. Scheutjens, T. Cosgrove, and B. Vincent, (Chapman and Hall, Bristol, 1993).
[2] *Polymer Brushes: Synthesis, Characterization, Applications*, edited by R. C. Advincula, W. J. Brittain, K. C. Caster, and J. Rühe, (Wiley, Weinheim, 2004).
[3] B. Zhao and W. J. Brittain, Prog. Polym. Sci. **25**, 677 (2000).
[4] W. J. Brittain and S. Minko, J. Polym. Sci. A **45**, 3505 (2007).
[5] J. Ruhe, M. Ballauff, M. Biesalski, P. Dziezok, F. Grohn, D. Johannsmann, N. Houbenov, N. Hugenberg, R. Konradi, S. Minko, M. Motornov, R. R. Netz, M. Schmidt, C. Seidel, M. Stamm, T. Stephan, D. Usov, and H. N. Zhang, Adv. Polym. Sci. **165**, 79 (2004).
[6] H. J. Tauton, C. Toprakcioglu, L. J. Fetters, and J. Klein, Nature (London) **332**, 712 (1988).
[7] P. Auroy, L. Auvray, and L. Leger, Phys. Rev. Lett. **66**, 719 (1991).
[8] A. Karim, S. K. Satija, J. F. Douglas, J. F. Anker, and L. J. Fetters, Phys. Rev. Lett. **73**, 3407 (1994).
[9] M. Manghi, M. Aubouy, C. Gay, and C. Ligoure, Eur. Phys. J. E **5**, 519 (2001).
[10] K. Prochazka, J. Phys. Chem. **99**, 14108 (1995).
[11] E. B. Zhulina, T. M. Birshtein, and O. V. Borisov, Eur. Phys. J. E **20**, 243 (2006).
[12] D. Dimitrov, A. Milchev, and K. Binder, Macromol. Symp. **252**, 47 (2007).
[13] D. Dimitrov, A. Milchev, and K. Binder, J. Chem. Phys. **125**, 034905 (2006).
[14] D. Dimitrov, A. Milchev, K. Binder, and D. W. Heermann, Macromol. Theory Simul. **15**, 573 (2006).
[15] P. G. de Gennes, *Scaling Concepts in Polymer Physics* (Cornell University Press, Ithaca, 1979).
[16] K. Kremer and K. Binder, J. Chem. Phys. **81**, 6381 (1984).
[17] A. Milchev and K. Binder, J. Phys. II **6**, 21 (1996).
[18] K. Avramova and A. Milchev, J. Chem. Phys. **124**, 024909 (2006).
[19] S. B. Chen, J. Chem. Phys. **123**, 074702 (2005).
[20] I. Teraoka and Y. Wang, Polymer **45**, 3835 (2004); G. F. Hermsen, M. Wessling, and N. F. A. van der Vegt, *ibid.* **45**, 3027 (2004).
[21] D. I. Dimitrov, A. Milchev, K. Binder, L. I. Klushin, and A. M. Skvortsov, J. Chem. Phys. **128**, 234902 (2008).
[22] C. Ligoure and L. Leibler, Macromolecules **23**, 5044 (1990).
[23] T. A. Witten and P. A. Pincus, Macromolecules **19**, 2509 (1986).
[24] J. Grumelard, A. Taubert, and W. Meier, Chem. Commun. (Cambridge) **2004**, 1642.
[25] F. Tessier and G. W. Slater, Macromolecules **39**, 1250 (2006).
[26] E. M. Sevick, Macromolecules **29**, 6952 (1996).
[27] S. Alexander, J. Phys. (Paris) **37**, 1443 (1976).
[28] P. G. de Gennes, Macromolecules **13**, 1069 (1980).
[29] M. Daoud and J. P. Cotton, J. Phys. (Paris) **43**, 531 (1982).
[30] C. B. Gorman, R. J. Petrie, and J. Genzer, Macromolecules **41**, 4856 (2008).
[31] A. G. Koutsioubas, N. Spiliopoulos, D. L. Anastassopoulos, A. A. Vradis, and G. D. Priftis, J. Appl. Phys. **103**, 094521 (2008).
[32] I. Carmesin and K. Kremer, Macromolecules **21**, 2819 (1988).
[33] P.-Y. Lai and K. Binder, J. Chem. Phys. **95**, 9258 (1991).
[34] P.-Y. Lai and K. Binder, J. Chem. Phys. **97**, 586 (1992).
[35] J. Wittmer, A. Johner, J. F. Joanny, and K. Binder, J. Chem. Phys. **101**, 4379 (1994).
[36] A. G. Koutsioubas and A. G. Vanakaras, Langmuir **24**, 13717 (2008).
[37] L.-C. Jia and P.-Y. Lai, J. Chem. Phys. **105**, 11319 (1996).
[38] G. D. Smith, Y. Zhang, F. Yin, D. Bedrov, M. D. Dadmun, and Z. Huang, Langmuir **22**, 664 (2006).
[39] P.-Y. Lai, J. Chem. Phys. **98**, 669 (1993).
[40] I. Hiotelis, A. G. Koutsioubas, N. Spiliopoulos, D. L. Anastassopoulos, A. A. Vradis, C. Toprakcioglu, A. Menelle, G. Sakellariou, and N. Hadjichristidis, Macromolecules **41**, 7648 (2008).
[41] A. M. Rubio, M. Storey, J. Felicity, M. Lodge, and J. J. Freire, Macromol. Theory Simul. **11**, 171 (2002).
[42] H. P. Deutsch and K. Binder, J. Chem. Phys. **94**, 2294 (1991).
[43] L. I. Klushin, A. M. Skvortsov, H.-P. Hsu, and K. Binder, Macromolecules **41**, 5890 (2008).
[44] W. Reisner, K. J. Morton, R. Riehn, Y. M. Wang, Z. Yu, M. Rosen, J. C. Sturm, S. Y. Chou, E. Frey, and R. H. Austin, Phys. Rev. Lett. **94**, 196101 (2005).
[45] A. Milchev, K. Binder, and A. Bhattacharya, J. Chem. Phys. **121**, 6042 (2004).
[46] C. T. A. Wong and M. Muthukumar, J. Chem. Phys. **128**, 154903 (2008).
[47] K. To, P.-Y. Lai, and H. K. Pak, Phys. Rev. Lett. **86**, 71 (2001).
[48] K. To and P.-Y. Lai, Phys. Rev. E **66**, 011308 (2002).